Poincaré covariant particle dynamics. II. Fragmentation for ultrarelativistic reactions

D. Behrens, G. Peter,* and C. C. Noack
Institut für Theoretische Physik, Universität Bremen, D–28334 Bremen, Germany
(Received 12 January 1994)

We present a Poincaré covariant model for ultrarelativistic particle reactions without any field degrees of freedom. A relativistic two-particle interaction is made possible by an enlargement of phase space and a distinction between physical and canonical particle coordinates. A Hamiltonian formalism with a mass-like quasipotential defines the dynamics of the system. Then interaction at a distance causes a change of effective particle masses instead of energy. Particle production is incorporated by a phenomenological decay procedure for the constituents (partons) in a manner analogous to a string fragmentation mechanism. This pure particle picture for Poincaré covariant collision dynamics (PCD model) is compared to other microscopic models and tested by simulations of e^+e^- jet events. Before application to more complex scenarios like ultrarelativistic heavy ion collisions, hard gluonic effects should be included. In the PCD model, this can be done by introduction of massive gluons as particles.

PACS number(s): 25.75.+r, 03.30.+p, 24.10.Jv, 13.65.+i

I. INTRODUCTION

The existence of the quark gluon plasma (QGP) as a real state of nuclear matter is still a question under intense research [1]. Neither the experimental nor the theoretical situation can be viewed as satisfactory. The basic equations of QCD are as yet unsolved for complex dynamical situations as in ultrarelativistic nucleus-nucleus reactions. Hence several models have been developed to establish the link between fundamental theory and physical observables. At the same time, the idea that the formation of a QGP would reveal itself by simple unique signatures has not been verified in present heavy ion experiments. Observed effects like strangeness enhancement or J/ψ suppression can be explained via QGP formation, but equally well in purely hadronic scenarios. To detect an eventual plasma formation, experimental efforts tend to even higher energies and larger nuclei, and theory has to keep up by detailed construction of reliable models that include all possible hadronic processes.

Several microscopic models, e.g., the Lund model (FRITIOF) [2,3], VENUS [4], relativistic quantum molecular dynamics (RQMD) [5], or the string gas model [6,7], have been developed to cover the hadronic aspects in ultrarelativistic nucleus-nucleus collisions. Except for RQMD they all treat the particle dynamics inconsistently because use of the correct kinematics (in the form of the relativistic energy-momentum relation) alone does not provide a Poincaré covariant description. Any sequence of nonlocal events found during a collision does depend on the frame of reference, and so do the results [8]. While this seems not to be a serious deficiency at Lawrence Berkeley BEVALAC energies, the influence of space-time structure will increase with energy and the number of hadrons involved.

Unfortunately, the formulation of relativistic particle dynamics is notoriously stubborn from the very beginning. While a (local) nonrelativistic field theory, due to the locality of interactions, can well be generalized to the relativistic case, the no-interaction-theorem [9] inhibits a straightforward relativistic extension of Hamiltonian dynamics where N particles interact instantaneously via potentials. One possible way out, the enlargement of phase space to $8N$ dimensions, causes serious difficulties with respect to the physical interpretation in systems with $N > 2$. But if, as is usually done in relativistic heavy ion interactions, the whole description of the dynamics is in terms of separable two particle interactions, these difficulties can be resolved uniquely. This Poincaré covariant approach was succesfully applied to heavy ion reactions at BEVALAC energies [10,11] where pion production was incorporated by a phenomenological creation process via Δ resonances.

For ultrarelativistic heavy ion reactions, a similar approach for particle dynamics was taken in Ref. [5]. These models, however, describe particle production within the framework of string dynamics [12] and an appropriate string decay mechanism. In contrast, we have formulated a model that retains the particle picture consistently for the fragmentation of a highly excited, strongly interacting pair of partons. This combination of particle dynamics and fragmentation scheme we call PCD (Poincaré covariant collision dynamics). The model consistently describes all subprocesses involved in ultrarelativistic reactions on the basis of point particles that obey relativistic Hamiltonian dynamics.

The principles of PCD for pointlike particles interacting at a distance are summarized in Sec. II. The two-

*Now at Fraunhofer-Institut für Angewandte Materialforschung, D–28717 Bremen, Germany.

particle case is sufficient because we deal only with quark-antiquark and quark-diquark subsystems. In Sec. III we describe a stable and a fragmenting hadron as a pair of interacting partons. Confinement is enforced by a quasipotential, and the excess of effective particle masses determines the decay. Our fragmentation scheme is verified in Sec. IV by comparing fragmentation functions of different models and simulations of jet events in e^+e^- collisions.

II. POINCARÉ COVARIANT HAMILTONIAN DYNAMICS

In our approach,[1] the dynamics of two interacting relativistic particles in the absence of any further (field) degrees of freedom is described in terms of a Poincaré covariant Hamiltonian:

$$H = \sum_{i=1}^{2} \frac{m_i^2 - p_i^2}{2m_i} + V(x_1, x_2, p_1, p_2) \,. \tag{2.1}$$

Here the four-vectors ${x_i}^\mu = (t_i, \mathbf{x}_i)$ and ${p_i}^\mu = (E_i, \mathbf{p}_i)$ $(i = 1, 2)$ represent the canonically conjugate coordinates and momenta of the particles, and the m_i are their masses. Note that the Hamiltonian H and the quasipotential V are *masslike* Lorentz scalars, the single-particle time coordinates t_i and energies E_i are *dynamical variables* of the system, and the total energy $E = E_1 + E_2$ is *different from* H. Furthermore, we have to distinguish the mass parameters m_i from effective masses $M_i := \sqrt{p_i^2}$. Phase space trajectories are parametrized by an additional Lorentz scalar evolution parameter τ which controls the development of the system via Hamilton's equations:

$$\dot{x}_i := \frac{dx_i}{d\tau} = \{H, x_i\}, \quad \dot{p}_i := \frac{dp_i}{d\tau} = \{H, p_i\} \,. \tag{2.2}$$

To establish a physical interpretation, a unique connection between τ and the observer time in any given reference frame is required.

The canonical transformation

$$y := (y_0, \mathbf{y}) := (m_1 x_1 + m_2 x_2)/m \,, \tag{2.3a}$$
$$p := (E, \mathbf{p}) := p_1 + p_2 \,, \tag{2.3b}$$
$$x := (x_0, \mathbf{r}) := x_1 - x_2 \,, \tag{2.3c}$$
$$q := (q_0, \mathbf{q}) := \mu\,(p_1/m_1 - p_2/m_2) \tag{2.3d}$$

[where $m := m_1 + m_2$ and $\mu := (m_1 m_2)/m$ are the total and reduced mass of the system] defines center-of-mass (c.m.) and relative coordinates in the usual way. The two-particle Hamiltonian (2.1) then reads

$$H = \frac{m^2 - p^2}{2m} - \frac{q^2}{2\mu} + V(\hat{x}) \,, \tag{2.4}$$

where we have restricted the quasipotential V to depend only on the component of the relative coordinate x orthogonal to the total momentum:

$$\hat{x} \equiv x_\perp := x - \frac{xp}{p^2}\, p \,. \tag{2.5}$$

In the c.m. system, it is independent of time, and connected to the spatial distance by $\sqrt{-\hat{x}^2} = |\mathbf{r}^{\text{c.m.}}|$. The reason for this restriction is to guarantee a simple physical solution for the effective particle masses,

$$p_i^2 = m_i^2 + 2\mu V \,. \tag{2.6}$$

Thus particles will always be on their mass shell ($M_i = \sqrt{p_i^2} = m_i$) in regions where $V = 0$, regardless of what their interaction might be in other regions of phase space.

The dependence of the quasipotential V on the total momentum p implies that the canonical coordinate y cannot be interpreted as representing the physical c.m., since $\mathbf{y}^{\text{c.m.}}$ is not at rest whenever $V(\hat{x})$ is not constant. Consequently we have to distinguish *canonical* from *physical* coordinates. We do this by *defining* a new physical c.m. coordinate

$$z := (z_0, \mathbf{z}) := y + \frac{qp}{p^2}\, x - \frac{xp}{p^2}\, q \,. \tag{2.7}$$

This definition entails the following equations of motion:

$$\dot{z} = p/m \,, \tag{2.8a}$$
$$\dot{p} = 0 \,, \tag{2.8b}$$
$$\dot{x} = q/\mu \,, \tag{2.8c}$$
$$\dot{q} = 2V'\hat{x} \,, \tag{2.8d}$$

where $V' := dV/d\hat{x}^2$ was introduced. It is seen from (2.8) that z behaves as a c.m. coordinate should, and, in particular, its zeroth component in the c.m. system can be used to establish a unique connection between the Lorentz scalar τ and an observer time $T_{\text{obs}}^{\text{c.m.}}$:

$$T_{\text{obs}}^{\text{c.m.}} := z_0^{\text{c.m.}} = (E^{\text{c.m.}}/m)\,\tau \,. \tag{2.9}$$

Finally, the physical single-particle coordinates are given by $z_i := z \pm (\mu/m_i)\, x$.

III. PCD MODEL OF THE PARTON-PARTON INTERACTION

Whereas in conventional string models the interaction of a highly excited pair of partons is simulated by energy exchange via a (1+1)-dimensional classical field, the corresponding PCD interaction uses an appropriate quasipotential which changes the effective parton masses. In this section we discuss a confinement quasipotential, leading to constant momentum change for the partons (Sec. III A), and give the solution of the equations of motion in (1+1) dimensions (Sec. III B). Finally, a consistent formulation of the fragmentation process is incorporated to the interaction model (Secs. III C–III E).

[1] A more detailed description can be found in [11].

A. The confinement model

To simulate confinement of two partons interacting at a distance, we choose the quasipotential V as a linear function of the spatial parton distance in the c.m. system. Its strength is fixed by a Lorentz scalar $\tilde{\kappa}$:

$$V(\hat{x}^2) = \tilde{\kappa}\sqrt{-\hat{x}^2} = \tilde{\kappa}\,|\mathbf{r}^{\text{c.m.}}| \,. \tag{3.1}$$

Selecting the c.m. system for our considerations, the equations of motions (2.8) in (1+1) space-time dimensions[2] read explicitly

$$\dot{z}_0 = \frac{E}{m}, \quad \dot{z} = 0 \,, \tag{3.2a}$$

$$\dot{E} = 0 \,, \quad \dot{p} = 0 \,, \tag{3.2b}$$

$$\dot{x}_0 = \frac{q_0}{\mu}, \quad \dot{x} = \frac{q}{\mu} \,, \tag{3.2c}$$

$$\dot{q}_0 = 0 \,, \quad \dot{q} = -[\operatorname{sgn} x]\,\tilde{\kappa} \,. \tag{3.2d}$$

As a first consequence we observe the linear connection between the single-particle momentum and observation time:

$$\frac{dp_i}{dT_{\text{obs}}} = \pm\frac{\dot{q}}{\dot{z}_0} = \mp[\operatorname{sgn} x]\,\tilde{\kappa}\,\frac{m}{E} \,. \tag{3.3}$$

A similar result in (1+1) dimensions is found in classical string models [12] with underlying noncovariant Hamiltonian, depending on end-point variables x_i and p_i,

$$H = E = \sqrt{m_1^2 + p_1^2} + \sqrt{m_2^2 + p_2^2} + \kappa\,|x_1 - x_2| \,. \tag{3.4}$$

The last term sometimes is interpreted as a potential proportional to the distance between the interacting particles, ignoring the field degrees of freedom as true origin of the interaction. Applying ordinary Hamilton's equations leads to

$$\frac{dp_i}{dT_{\text{obs}}} = \mp[\operatorname{sgn}(x_1 - x_2)]\,\kappa \tag{3.5}$$

for the end points of the string.

We may compare both models if we relate our quasipotential strength $\tilde{\kappa}$ to the string tension κ by

$$\frac{m}{E}\,\tilde{\kappa} = \kappa \,, \tag{3.6}$$

where E and m are the total energy and mass of the two-parton system. Then the resulting periodic evolution of individual momenta in the c.m. system is identical in both models [cf. Figs. 1(a) and 1(b)].

B. Yo-yo solution in (1+1) dimensions

By direct integration of (3.2) we obtain the complete solution for a q-$\bar{q}$ system[3] at rest. For a half period [$s := \operatorname{sgn} x = \text{const}$],

$$z_0 = \frac{E}{m}(\tau - \tau_0) + z_0(\tau_0), \quad z = 0 \,, \tag{3.7a}$$

$$E = \text{const}, \quad p = 0 \,, \tag{3.7b}$$

$$x_0 = \frac{q_0}{\mu}(\tau - \tau_0) + x_0(\tau_0) \tag{3.7c}$$

$$x = -s\,\frac{\tilde{\kappa}}{2\mu}(\tau - \tau_0)^2 + \frac{q(\tau_0)}{\mu}(\tau - \tau_0) + x(\tau_0) \,,$$

$$q_0 = \text{const}, \quad q = -s\,\tilde{\kappa}\,(\tau - \tau_0) + q(\tau_0) \,. \tag{3.7d}$$

It has to be mentioned that $E = E_1 + E_2$ and $q_0 = \mu(E_1/m_1 - E_2/m_2)$ are not independent initial conditions but are connected to $x(\tau_0)$ and $q(\tau_0)$ to guarantee (2.6):

$$E_i = \sqrt{m_i^2 + q^2(\tau_0) + 2\mu\tilde{\kappa}s\,x(\tau_0)} \,. \tag{3.8}$$

While the single-particle energies $E_i = Em_i/m \pm q_0$ are constant, the effective parton masses vary periodically:

$$M_i(\tau) = \sqrt{E_i^2 - p_i^2(\tau)} = \sqrt{m_i^2 + 2\mu\tilde{\kappa}s\,x(\tau)} \,. \tag{3.9}$$

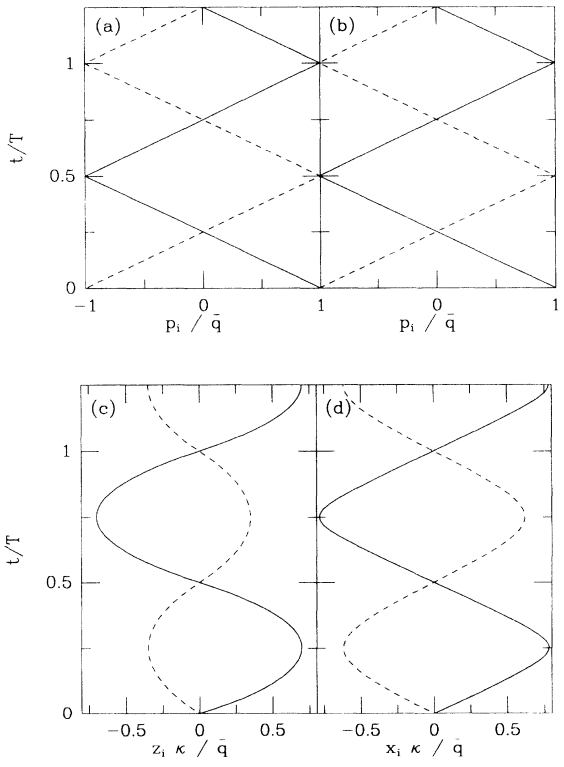

FIG. 1. Particle (left) vs string picture (right): Evolution in observer time (t) of momenta (a,b) and coordinates (c,d) of two confined partons in their c.m. system. For both cases the momenta change linearly with an amplitude $\bar{q}$ and a time period $T = 4\bar{q}/\kappa$. In the particle picture the physical (not canonical) single-particle coordinates (z_i) follow branches of parabolas. In the string picture physical (and canonical) coordinates ($x_i \equiv z_i$) are of hyperbolic shape [$m_1 = \bar{q}/4$ (—), $m_2 = 2m_1$ (- - -)].

[2]To simplify notation, the former symbols for the four-vectors (x,p,...) from now on denote the spatial components of "two-vectors."

[3]We refer to the q-$\bar{q}$ system only, but everything is valid for the q-qq system as well.

The τ period of the (yo-yo) movement is found from the condition $x(\tau) = 0$ to be $\tau^* = 4\bar{q}/\tilde{\kappa}$, where $\bar{q}$ is the maximum relative momentum:

$$\bar{q} = \max_{\tau} |q(\tau)| = \sqrt{q^2(\tau_0) + 2\mu\tilde{\kappa}s\, x(\tau_0)} \ . \qquad (3.10)$$

Observation time ($T_{\rm obs}$) is equal to the c.m. system time (z_0), and, because of the linear connection to evolution parameter τ, the parton motion eventually can be parametrized by $T_{\rm obs}$.

As stated before, the single-parton momenta change linearly with observation time [Fig. 1(a)]. The spatial trajectories of physical coordinates (z_i) consist of smoothly connected branches of parabolas [Fig. 1(c)]. This is different in the string picture [12], where hyperbolic solutions are found for the single-particle coordinates x_i [Fig. 1(d)]. For massless partons ($m_i \to 0$) they approach straight lines, whereas they remain parabolic in the particle picture.

From Figs. 2(a–d) the main differences for the yo-yo mode between particle and string picture can be seen. The single-particle energy is constant throughout in the particle picture [Fig. 2(a)]. In the string picture, the energy is exchanged between both end points via the classical string field [Fig. 2(b)]. Conversely, the effective single-particle masses in the particle picture [Fig. 2(c)] vary between their minimum and maximum values ($\underline{M_i} = m_i$, $\overline{M_i} = \sqrt{m_i^2 + \bar{q}^2}$), whereas the end points of the string [Fig. 2(d)] always stay on the mass shell ($\sqrt{E_i^2 - p_i^2} = m_i$).

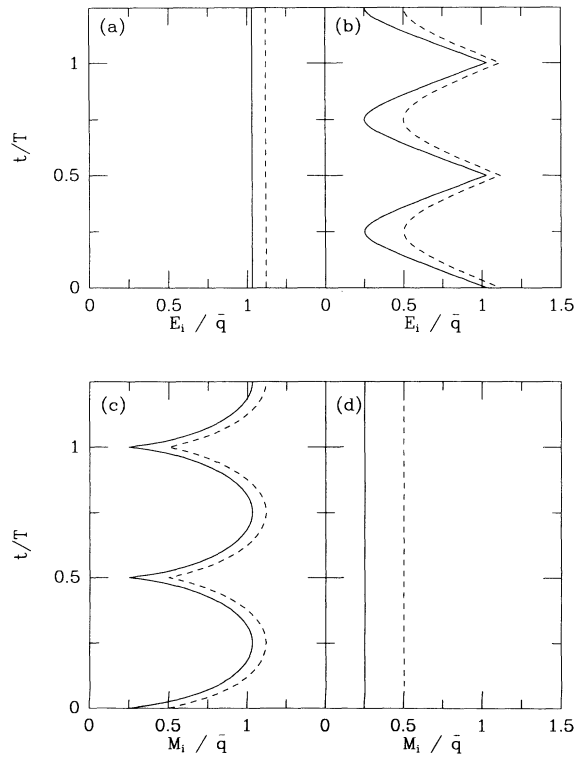

FIG. 2. Particle (left) vs string picture (right): Evolution of energies (a,b) and effective masses (c,d) of the same two parton system as in Fig. 1.

C. Covariant fragmentation

Because the two-parton system subjected to the linear quasipotential is unconditionally stable, we have to introduce an additional process for particle production (hadronization). As for the origin of particle creation we use the growing effective masses of interacting partons. Since the motion of a highly excited quark-antiquark pair is restricted essentially to one spatial (longitudinal) dimension, we can apply the (1+1)-dimensional equations of motion with analytical yo-yo solutions in that case. Assuming a sufficiently large initial relative momentum, the partons, while separating, may obtain masses large enough so that a "parton decay" (quark-antiquark creation) becomes kinematically possible. Since classical Hamilton theory does not allow for particle production, a specific parton decay law (Sec. III D) must be added to our model to specify the moment (τ point) of fragmentation.

We illustrate particle production in the PCD model by a fragmenting quark q_1 interacting with antiquark $\bar{q}_1$. The production of a new quark-antiquark pair $q_2\bar{q}_2$ can be symbolized by

$$(\bar{q}_1\text{-}q_1) \to (\bar{q}_1'\text{-}q_2) + (\bar{q}_2 q_1') \ , \qquad (3.11)$$

where parentheses indicate a color singlet and a hyphen connects partons with enough relative momentum to undergo further fragmentation. The primes indicate that neither of the primary partons remains in its initial state. In particular, energy and momentum of the original antiquark $\bar{q}_1$ are affected by the decay of q_1 into q_2 and $(\bar{q}_2 q_1') =: h$. The created antiquark $\bar{q}_2$ together with the quark q_1' are coupled to a stable on-mass-shell meson ($m_h^2 = E_h^2 - \mathbf{p}_h^2$), while the newly formed $(\bar{q}_1'\text{-}q_2)$ state is not necessarily a physical hadron. This would be the other way around if the original antiquark $\bar{q}_1$ is responsible for the pair production.

After fragmentation we need to know momentum and energy (or effective mass) of the three particles $\bar{q}_1'$, q_2, and h. In what follows, most of these variables will be fixed, but the momentum of the meson is kept as a free parameter. The way we choose it is discussed in Sec. III E. Here we use $\mathbf{p}_h$ to represent the meson momentum in the rest frame of the decaying quark q_1.

On the basis of a simple two-particle decay ($q_1 \to q_2 + h$) we calculate the effective mass M_2 of the quark q_2 :

$$M_2^2 = M_1^2 - 2M_1\sqrt{m_h^2 + \mathbf{p}_h^2} + m_h^2 \ . \qquad (3.12)$$

M_2 is restricted by the bare mass m_2 and the effective mass of the decaying quark q_1 ($M_1 = \sqrt{E_1^2 - \mathbf{p}_1^2}$) :

$$m_2 \le M_2 \le M_1 - m_h \ . \qquad (3.13)$$

Because of the interaction with q_2 the effective mass of $\bar{q}_1'$

is fixed by (2.6) :

$$M_{\bar{1}}'^2 = m_{\bar{1}}^2 + (M_2^2 - m_2^2) \,. \tag{3.14}$$

Finally, in the c.m. system of the diverging ($\bar{q}_1'$-q_2)-pair we have

$$|\mathbf{p}_{\bar{1}}'| = |\mathbf{p}_2| = \frac{1}{2M'} \sqrt{\lambda(M'^2, M_{\bar{1}}'^2, M_2^2)} \,, \tag{3.15}$$

where $\lambda(a^2, b^2, c^2) := [a^2 - (b+c)^2][a^2 - (b-c)^2]$. In this same reference frame the direction of $\mathbf{p}_{\bar{1}}'$ is selected to coincide with that of $\mathbf{p}_{\bar{1}}$. The effective mass M' of the next-generation confined quark-antiquark pair ($\bar{q}_1'$-q_2) is connected to the initial effective mass M of the original ($\bar{q}_1$-q_1) system by

$$M'^2 = M^2 - 2\,\frac{M}{M_1}\left\{E_1 \sqrt{m_h^2 + \mathbf{p}_h^2} + \mathbf{p}_1 \cdot \mathbf{p}_h\right\} + m_h^2 \,. \tag{3.16}$$

Note that $(E_1, \mathbf{p}_1)$ refers to the c.m. system of ($\bar{q}_1$-q_1) and $\mathbf{p}_h$ to the rest frame of q_1, while (3.15) fixes $\mathbf{p}_{\bar{1}}'$ and $\mathbf{p}_2$ in the c.m. system of ($\bar{q}_1'$-q_2). As long as enough relative momentum is left in the system to realize

$$M_1 > m_2 + m_h \tag{3.17}$$

for the decaying parton, we may proceed with hadron production.

A realistic parton fragmentation model would also need a prescription for fixing flavor and spin in the newly created quark-antiquark pair. These degrees of freedom can be taken into account, as in other models, by introducing further parameters. Here we assume for simplicity the existence of just one flavor with corresponding low parton mass. As a consequence, all mesons created in our simple fragmentation cascade appear as pions.

D. Parton decay law

The probability distribution used to determine the moment (τ point) for the decay of a parton closely follows the area law for the fragmentation of a classical string [13]. In the string model,

$$dP(A) = \Lambda \exp(-\Lambda\, A)\, dA \tag{3.18}$$

provides the probability for the string to break after a world sheet A is swept out undisturbedly. The decay constant Λ, which can be approximated from QCD [6], is usually fixed by a fit to experimental data. For a massless string, the swept-out area A is related to the string energy E by

$$A = \frac{E^2}{4\,\kappa^2} \,. \tag{3.19}$$

In this string picture, a linear decrease of relative momentum in the quark-antiquark system is connected to an increase of string energy. In the PCD model we have a growth of the effective masses instead. Hence, we adapt Eq. (3.18) by replacing string energy E with effective mass M_i of the parton:

$$dP = \Lambda \exp\left(-\Lambda\,\frac{M_i^2}{4\,\kappa^2}\right) d\left(\frac{M_i^2}{4\,\kappa^2}\right) =: g(M_i)\, dM_i \,. \tag{3.20}$$

Then the probability for a parton to decay with effective mass M_i is given by the distribution function

$$g(M_i) = N\,\frac{M_i}{M_0^2} \exp\left(-\frac{M_i^2}{2\,M_0^2}\right) \,. \tag{3.21}$$

The normalization (N) depends on the actually available interval for the effective mass M_i. The most probable effective mass for the creation of a quark-antiquark pair,

$$M_0 := \sqrt{2/\Lambda}\,\kappa \,, \tag{3.22}$$

is (just as Λ in the string case) in principle a free parameter of the model, which will be fitted to the experimentally observed distributions of particles. Using Λ as estimated from the pair creation probability in a homogeneous chromoelectrical field of the flux tube between quark and antiquark [6], we would have $M_0 \approx 1$ GeV.

E. Meson momentum distribution

In order to determine the distribution of energy and momentum among the fragments, we simplified the production process (3.11) to a two-body decay of quark q_1 into quark q_2 and meson h without inner degrees of freedom. Energy and momentum of the decay products are still not uniquely determined. In the PCD model we fix the meson momentum by employing a probability distribution for $\mathbf{p}_h$ in the rest frame of q_1. The maximum magnitude is found from the masses of the particles involved. From $|\mathbf{p}_h| = \sqrt{\lambda(M_1^2, M_2^2, m_h^2)}\,/2M_1$ we obtain, using (3.13) [with λ as in (3.15)] :

$$|\mathbf{p}_h| \le p_{\max} := \frac{1}{2M_1} \sqrt{\lambda(M_1^2, m_2^2, m_h^2)} \,. \tag{3.23}$$

Now we assume an isotropic distribution of meson momentum $\mathbf{p}_h$. Two alternatives will be considered. The first one is homogeneous and isotropic in the available three-dimensional momentum space (marked by PCD_1) :

$$dP = f_{3\mathrm{D}}(\mathbf{p}_h)\, d^3p_h \sim d^3p_h \,. \tag{3.24}$$

The second one (PCD_2) is homogeneous and isotropic in four momentum space, but with a δ function restricting to on-mass-shell mesons:

$$dP = f_{4\mathrm{D}}(\mathbf{p}_h)\, d^3p_h \sim d^3p_h \int_0^\infty dE_h\, \delta(E_h^2 - \mathbf{p}_h^2 - m_h^2) \sim d^3p_h / \sqrt{m_h^2 + \mathbf{p}_h^2} \,. \tag{3.25}$$

The distribution functions are normalized in the sphere of possible meson momenta: $S(p_{\max}) := \{|\mathbf{p}_h| \le p_{\max}\}$. Hence, we have

$$f_{3\mathrm{D}}^{-1}(\mathbf{p}_h) = \tfrac{4}{3}\,\pi\, p_{\max}^3 \tag{3.26}$$

and

$$f_{4D}^{-1}(\mathbf{p}_h) = 2\pi\sqrt{m_h^2+\mathbf{p}_h^2} \times \left(p_{\max}\sqrt{m_h^2+p_{\max}^2} - m_h^2 \operatorname{arcsinh}\frac{p_{\max}}{m_h}\right) . \quad (3.27)$$

Once the meson momentum $\mathbf{p}_h$ is selected from one of the above distributions, all remaining kinematical variables are uniquely fixed, and the PCD fragmentation process is completed.

IV. MODEL DISCUSSION

Before integrating the PCD model developed so far into a more complex scenario like ultrarelativistic heavy ion collisions, we tested its credibility in two aspects. The fragmentation function $f(z)$, representing the single fragmentation process, is compared to other models, and a set of calculated jet events is qualitatively compared with experimental results.

A. Fragmentation function

Fragmentation usually is a process where one spatial direction is predominant. This one is called longitudinal, and in our case it is fixed by the diverging ($\bar{q}_1$-q_1) pair. Produced hadrons are classified by their energy-momentum content $[E_h + p_{h\parallel}]$ with respect to this direction $[p_{h\parallel} = |\mathbf{p}_h|\cos\vartheta]$. The function $f(z)$ gives the probability for the primary hadron to be provided with a portion z of the initial energy-momentum content of the fragmenting system. In the PCD model fragmentation means decay of the quark q_1. Hence, the ratio z, which is Lorentz invariant in the longitudinal direction, is given by

$$z = \frac{1}{W^+}\left(\sqrt{m_h^2+\mathbf{p}_h^2} + |\mathbf{p}_h|\cos\vartheta\right) , \quad (4.1)$$

where $W^+ = E_1(0)+|\mathbf{p}_1(0)|$ is the initial $[\tau = 0]$ energy-momentum of quark q_1. In the rest frame of q_1 we have

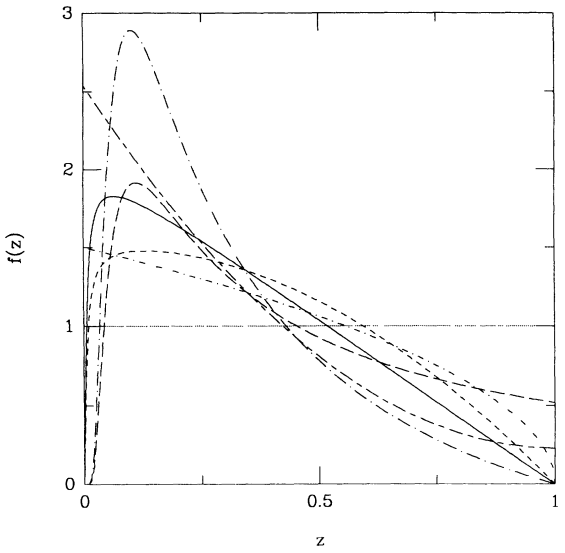

FIG. 3. Fragmentation function $f(z)$ of various models. For details see Table I.

$$W^+ = M_1\frac{E_1+\sqrt{E_1^2-m_q^2}}{E_1+\sqrt{E_1^2-M_1^2}} . \quad (4.2)$$

Here E_1 is the constant energy of the quark q_1 in the c.m. system of the ($\bar{q}_1$-q_1) pair, M_1 its τ-dependent effective mass, and m_q the initial bare mass $[M_1(0) = m_q]$.

Since in the PCD model the actual decay mass M_1 and hadron momentum $\mathbf{p}_h$ are selected from probability distributions (3.21) and (3.26) or (3.27), the fragmentation function $f(z)$ is found from all combinations of M_1 and $\mathbf{p}_h$ which lead to the given value of z:

$$f(z) \sim \int_{m_q+m_h}^{E_1} dM_1\, g(M_1) \times \int_{S(p_{\max})} d^3p_h\, f(\mathbf{p}_h)\,\delta\left(z - z(M_1,\mathbf{p}_h)\right) , \quad (4.3)$$

where $z(M_1,\mathbf{p}_h)$ is defined by (4.1) and (4.2). Note that the integrations are not interchangeable since the maximum hadron momentum $p_{\max}$ (3.23) is a function of the effective fragmentation mass M_1. In the large energy

TABLE I. Fragmentation function $f(z)$ of various models, where z is the fraction of initial energy-momentum. Except from the physical hadron mass m_h and the transverse mass $m_\perp = \sqrt{m_h^2+p_\perp^2}$, all other constants are appropriately chosen model parameters.

Model	$f(z)$	Ref.	In Fig. 3
Field-Feynman	$1-a+3a(1-z)^2$	[17]	— - — -
Simple Lund	1	[2]	.....
Standard Lund	$(1+c)(1-z)^c$	[2]	- · - · -
Symmetric Lund	$N_L(1-z)/z\exp(-b\,m_\perp^2/z)$	[2]	· — · — ·
VENUS	$N_V(1/z)\exp(-\Lambda\,m_h^2/z)$	[4]	— — —
PCD_1	$N_1(1-z^2)\exp(-m_h^2/2\,M_0^2\,z)$	(4.4a)	- - - - -
PCD_2	$N_2(1-z)\exp(-m_h^2/2\,M_0^2\,z)$	(4.4b)	———

limit [$E_1 \to \infty$] with zero bare quark mass [$m_q \to 0$] and small hadron mass [$m_h \ll M_0$], the fragmentation functions for our two different momentum distributions approach

$$[\mathrm{PCD}_1]: \qquad f_1(z) \sim (1-z^2)\exp\left(-\frac{m_h^2}{2M_0^2}\frac{1}{z}\right), \quad (4.4a)$$

$$[\mathrm{PCD}_2]: \qquad f_2(z) \sim (1-z)\exp\left(-\frac{m_h^2}{2M_0^2}\frac{1}{z}\right). \quad (4.4b)$$

They are included in Table I and Fig. 3, where fragmentation functions of various models are collected. Above $z = 0.1$ they all show a similar behavior. For smaller z values the functions for symmetric Lund, VENUS, and PCD rise exponentially as a consequence of the underlying exponential decay law of an exited classical string or the dressed parton, respectively. Summarizing, we find that our PCD fragmentation functions fit well into the spectrum of existing models. The steeper decrease of f_2 compared to f_1 favors production of pions with low energy-momentum, and thus causes somewhat higher multiplicities.

B. Numerical simulation

The comparison with experimental jet results is based on a Monte Carlo test of 5×10^4 simulated e^+e^- events in the PCD model. The jet axis was assumed to deviate from the ($\bar{q}_1$-q_1) direction by an angle that is Gaussian distributed with a width of 5°. Hadron (pion) mass $m_h = 0.14$ GeV, parton (u, d quark) mass $m_q = 0.01$ GeV, and string tension $\kappa = 1$ GeV were kept constant. The most probable decay mass then was adjusted to be $M_0 = 1.5$ GeV. For an estimate of the number of charged particles we used 2/3 of the total yields. Because low-energy effects such as resonance production or discrete mass spectra are not included in the PCD model, we only compare to experimental inclusive data above $W = 10$ GeV initial energy. In the PCD model W is the total energy of the initial ($\bar{q}_1$-q_1) pair in their c.m. system.

One characteristic of a jet event is the average charged multiplicity $\langle n_{\mathrm{ch}}\rangle$, which we calculated for both PCD model variants at four different initial energies (Fig. 4). As expected for our fragmentation model (which does not include hard QCD effects such as gluon bremsstrahlung), the multiplicities show a logarithmic increase with energy:

$$\langle n_{\mathrm{ch}}\rangle = a + b \ln s \quad (s := [W/(1\ \mathrm{GeV})]^2), \quad (4.5)$$

where $a = 2.56$, $b = 1.10$ for PCD_1 and $a = 2.48$, $b = 1.12$ for PCD_2. Consequently, the PCD model underestimates the charged multiplicities above $W = 30$ GeV where gluon emission becomes important.

The typical shape of the experimentally observed rapidity distributions dn_{ch}/dy consists of a plateau, broadening with initial energy W, and a steep decrease near the maximum value $y_{\max} \approx \ln(W/m_h)$. The overall structure is well reproduced in the PCD simulations (Fig. 5). The variants PCD_1 and PCD_2 merely differ in the height

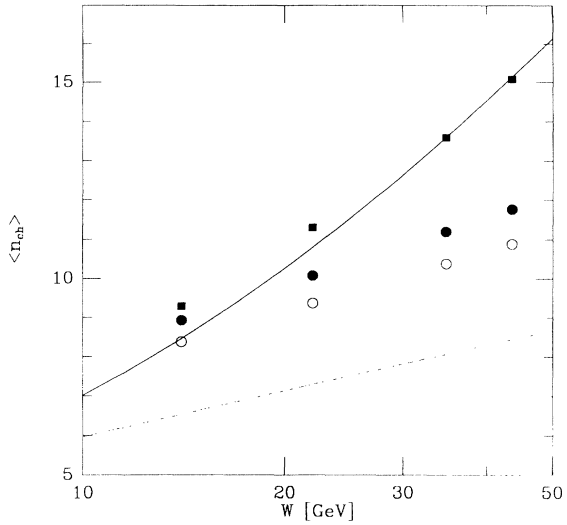

FIG. 4. Average charged multiplicity $\langle n_{\mathrm{ch}}\rangle$ as a function of jet energy W. The model predictions for PCD_1 (○) and PCD_2 (●) show an increase similar to the dotted line, an extrapolation of experimental low energy results ($W \lesssim 10$ GeV) [18]. The solid line represents a fit to experimental data (■) taking into account all energies [19].

of their (slightly inclined) plateaus. This difference is connected to the small deviation in multiplicity. We do not expect to reproduce the experimentally observed decrease for $y \to 0$ because gluon emission and production of heavier quarks [14] is not included in these simple PCD versions.

For the PCD model we also examined the composition of the rapidity plateau. We selected all 34 GeV jet events with exactly 15 particles in the final state, which is the

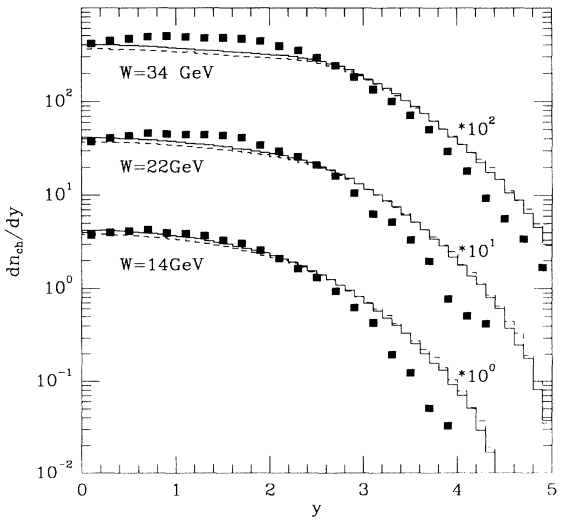

FIG. 5. Rapidity distributions of charged particles at different jet energies W. Squares represent experimental data [14], histograms show model results for PCD_1 (- - -) and PCD_2 (—). Particles from both jets are included.

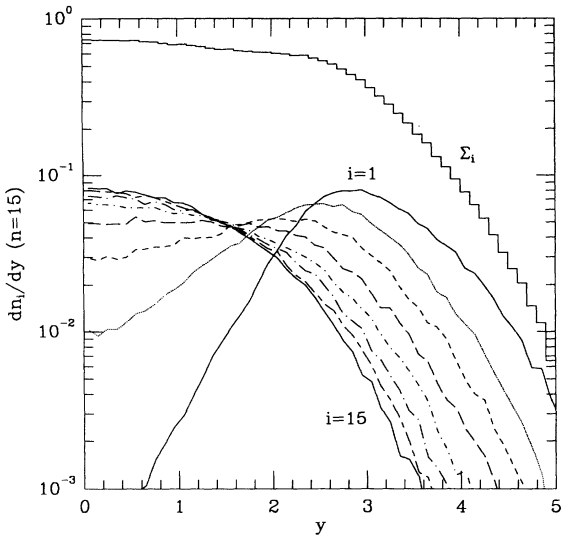

FIG. 6. One particle rapidity distributions ($i = 1, 3, 5, \ldots$) taken from all $W = 34$ GeV jet events with total multiplicity $n = 15$. The sum over all contributions also is shown.

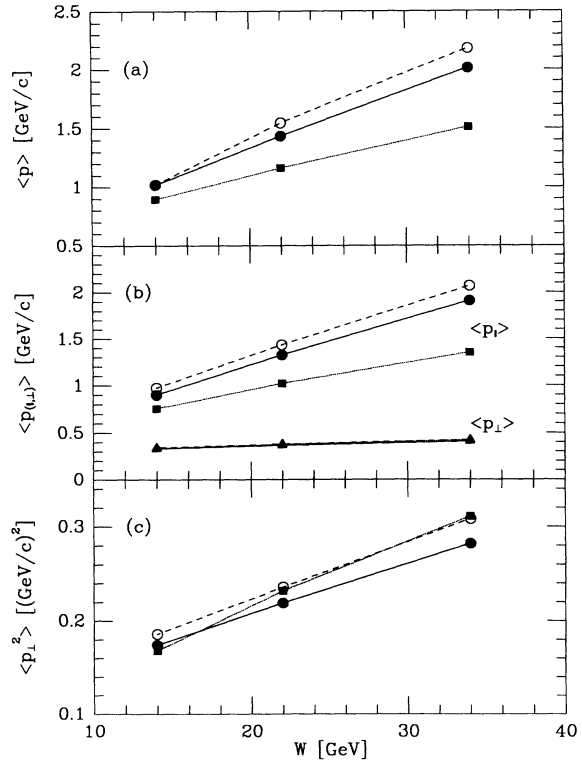

FIG. 7. Average magnitude of momenta $\langle p \rangle$ (a), longitudinal momenta $\langle p_\parallel \rangle$ (b), and squared transverse momenta $\langle p_\perp^2 \rangle$ (c) as functions of jet energy W. Symbol conventions as in Fig. 4. Lines just connect corresponding symbols. The triangles in (b) represent average transverse momenta $\langle p_\perp \rangle$, almost identical in model and experiment.

most probable total multiplicity in that case. The analysis with respect to successive particles (Fig. 6) shows that only the first few hadrons have a rapidity distribution with a maximum at nonzero rapidity. All others are distributed around a maximum at $y = 0$.

A matter of special interest is the comparison of experimental data and PCD prediction for the transverse hadron momentum $p_\perp$. At least for the primary hadron this distribution follows directly from (3.26) or (3.27) by integration:

$$f_1(p_\perp) = \int_{S(p_{\max})} d^3p\, f_{3D}(\mathbf{p})\, \delta(p_\perp - |\mathbf{p}| \sin\vartheta) = \frac{3p_\perp}{p_{\max}^2} \sqrt{1 - \left(\frac{p_\perp}{p_{\max}}\right)^2} \tag{4.6}$$

and analogously

$$f_2(p_\perp) = \frac{2p_\perp \operatorname{arccosh}\sqrt{(m_h^2 + p_{\max}^2)/(m_h^2 + p_\perp^2)}}{p_{\max}\sqrt{m_h^2 + p_{\max}^2} - m_h^2 \operatorname{arcsinh}\frac{p_{\max}}{m_h}} . \tag{4.7}$$

With growing initial energy W the decaying partons can achieve larger effective masses, and so the transverse momentum spectra depend on energy via $p_{\max}$. For increasing $p_{\max}$ these distributions broaden.

The results for e^+e^- jet simulations with initial energies $W = 14$, 22, and 34 GeV are shown in Fig. 7. The average transverse momentum $\langle p_\perp \rangle$ increases only slightly with energy [Fig. 7(b)]. This is in accordance with experiment. The average longitudinal momentum $\langle p_\parallel \rangle$ [Fig. 7(b)] and the average magnitude of the momentum $\langle p \rangle$ [Fig. 7(a)] increase even stronger than experimentally observed. This again is connected to the under-

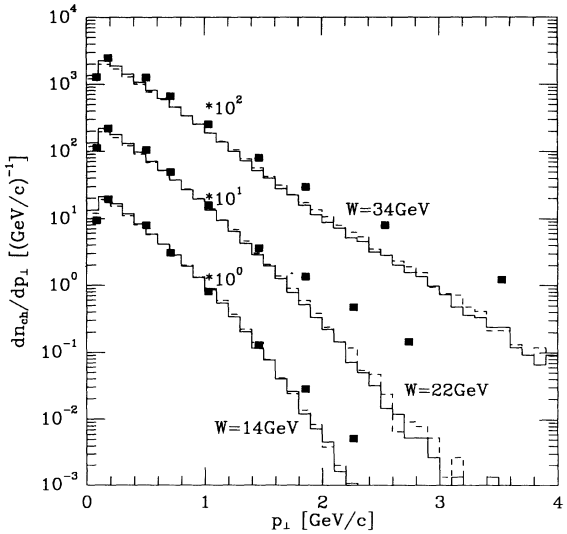

FIG. 8. Transverse momentum distributions of charged particles at different jet energies W. Symbol and line conventions as in Fig. 5.

estimated average multiplicities. The decreasing $\langle p_\perp/p_\parallel \rangle$ ratio in more energetic jets is then, of course, reproduced.

In addition we show the average squared transverse momentum $\langle p_\perp^2 \rangle$ [Fig. 7(c)]. The increase with energy explains the broadening of the transverse momentum spectra (Fig. 8). Except for the higher transverse momenta, the PCD variants both are in good agreement with the experimental distributions. We also reproduce the decrease at $p_\perp \to 0$, caused by limited phase space.

Hence, the multiplicities and the distributions of rapidity and momentum components found from PCD simulations are in general agreement with experimental results.

V. CONCLUSIONS

Within the framework of Poincaré covariant collision dynamics we have developed a two-parton interaction model for stable and nonstable color singlets. Confinement is simulated by a linear quasipotential which, in (1+1) dimensions, results in simple equations of motion, leading to parton dynamics with a somewhat damped space-time structure compared to string models [Figs. 1(c) and 1(d)]. The linear momentum change, a feature of both string and particle picture [Figs. 1(a) and 1(b)], causes complementary behavior of parton energies [Figs. 2(a) and 2(b)] and masses [Figs. 2(c) and 2(d)]. Whereas string end points exchange energy with the string field, PCD particles compensate a loss of momentum with an increase of effective mass in a quasipotential.

Fragmentation of a highly excited two-parton system is formulated consistently by a particle decay of one of the partons, provided sufficient effective mass is achieved during the interaction. The invariant decay mechanism is governed by a probability distribution similar to the area-breaking law in string models, and includes production of transverse momentum. Numerical results for e^+e^- jet events, though restricted in this paper to (stable) pions, show good agreement with experimental multiplicities, momentum and rapidity distributions.

Inclusion of further degrees of freedom to cover the whole spectrum of decay products is of no principle difficulty and can be effected either by introduction of additional model parameters or, alternatively, by applying phase-space arguments [15]. Likewise, hard perturbative gluon emission can be integrated in the PCD formalism by modeling a hard gluon as a massive particle interacting with the neighboring partons via separate two-particle quasipotentials. This concept has been explored for the ($\bar{q}_1$-G-q_1) system [16].

Encouraged by the results obtained so far, we feel that an extension of the model to ultrarelativistic heavy ion reactions is very promising. The power of PCD, the consistent Poincaré covariant description of all hadronic processes, including secondary interactions, should become even more important with respect to future experiments at yet higher energies and with heavier projectiles.

[1] *Proceedings of 8th Internatinal Conference on Ultra-Relativistic Nucleus-Nucleus Collisions (Quark Matter '90),* Menton [Nucl. Phys. **A525** (1991)], and references therein.

[2] B. Andersson, G. Gustafson, G. Ingelman, and T. Sjöstrand, Phys. Rep. **97**, 31 (1983).

[3] B. Andersson, G. Gustafson, and B. Nilsson-Almqvist, Nucl. Phys. **B281**, 289 (1987).

[4] K. Werner, Phys. Rep. **232**, 87 (1993).

[5] H. Sorge, H. Stöcker, and W. Greiner, Ann. Phys. (N.Y.) **192**, 266 (1989); Nucl. Phys. **A498**, 567c (1989).

[6] K. Sailer, B. Müller, and W. Greiner, Report No. UFTP 230/1989 (unpublished).

[7] K. Sailer, D. Neubauer, T.Schönfeld, B. Müller, and W. Greiner, in *The Nuclear Equation of State, Part B: QCD and the Formation of Quark-Gluon Plasma*, edited by W. Greiner and H. Stöcker, NASI Series B 216B (Plenum, New York, 1989), p. 531; K. Sailer, T. Schönfeld, Z. Schram, A. Schäfer, and W. Greiner, J. Phys. G **17**, 1005 (1991).

[8] T. Kodama, S. B. Duarte, K. C. Chung, R. Donangelo, and R. A. M. S. Nazareth, Phys. Rev. C **29**, 2146 (1984).

[9] D. G. Currie, T. F. Jordan, and E. C. G. Sudarshan, Rev. Mod. Phys. **35**, 350 (1963).

[10] G. Peter, Ph.D. thesis, Bremen, 1987.

[11] G. Peter, D. Behrens, and C. C. Noack, preceding paper, Phys. Rev. C **49**, 3253 (1994).

[12] X. Artru, Phys. Rep. **97**, 147 (1983).

[13] X. Artru and G. Mennessier, Nucl. Phys. **B70**, 93 (1974).

[14] TASSO Collaboration, M. Althoff *et al.*, Z. Phys. C **22**, 307 (1984).

[15] H. J. Schulze and J. Aichelin, Phys. Rev. D **43**, 2111 (1991).

[16] D. Behrens, C. C. Noack, G. Peter, Verh. DPG (VI) **26**, 554 (1991).

[17] R. D. Field and R. P. Feynman, Nucl. Phys. **B136**, 1 (1978).

[18] J. L. Siegrist *et al.*, Phys. Rev. D **26**, 969 (1986).

[19] TASSO Collaboration, W. Braunschweig *et al.*, Z. Phys. C **45**, 193 (1989).